A sodar for profiling in a spatially inhomogeneous urban environment

Meteorologische Zeitschrift, Vol. **24**, No. 6, 615–624 (published online November 5, 2015)

A sodar for profiling in a spatially inhomogeneous urban environment

Stuart Bradley[1*], Janet Barlow[2], John Lalley[2] and Christoforos Halois[2]

[1]University of Auckland, Auckland, New Zealand
[2]University of Reading, Reading, UK

(Manuscript received November 5, 2014; in revised form July 29, 2015; accepted July 29, 2015)

Abstract

The urban boundary layer, above the canopy, is still poorly understood. One of the challenges is obtaining data by sampling more than a few meters above the rooftops, given the spatial and temporal inhomogeneities in both horizontal and vertical. Sodars are generally useful tools for ground-based remote sensing of winds and turbulence, but rely on horizontal homogeneity (as do lidars) in building up 3-component wind vectors from sampling three or more spatially separated volumes. The time taken for sound to travel to a typical range of 200 m and back is also a limitation. A sodar of radically different design is investigated, aimed at addressing these problems. It has a single vertical transmitted sound pulse. Doppler shifted signals are received from a number of volumes around the periphery of the transmitted beam with microphones which each having tight angular sensitivity at zenith angles slightly off-vertical. The spatial spread of sampled volumes is therefore smaller. By having more receiver microphones than a conventional sodar, the effect of smaller zenith angle is offset. More rapid profiling is also possible with a single vertical transmitted beam, instead of the usual multiple beams.

A prototype design is described, together with initial field measurements. It is found that the beam forming using a single dish antenna and the drift of the sound pulse downwind both give rise to reduced performance compared with expectations. It is concluded that, while the new sodar works in principle, the compromises arising in the design mean that the expected advantages have not been realized

Keywords: Sodar accuracy, Doppler error, wind drift, acoustic dish antenna, urban wind measurement

1 Introduction

The design of conventional sodars relies on several narrow (typically ±3 ° beam-width) acoustic beams transmitted upward from the instrument (Bradley, 2007). Reception of sound scattered by turbulent refractive index fluctuations is from the same directions. If beam m is transmitted at zenith angle θ_m and at an azimuth angle ϕ_m with the x axis toward the East, then the radial velocity component contributing to Doppler shift is

$$\omega_m = u \sin\theta_m \cos\phi_m + v \sin\theta_m \sin\phi_m + w \cos\theta_m. \quad (1.1)$$

Including all M beams, the $M \times 1$ measurement matrix $\mathbf{\Omega}$ is given by

$$\mathbf{\Omega} = \mathbf{BV} \quad (1.2)$$

where the wind vector is $\mathbf{V} = (u, v, w)^T$. The least-squares solution of (1.2) is

$$\hat{\mathbf{V}} = (\mathbf{B}^T\mathbf{B})^{-1}\mathbf{B}^T\mathbf{\Omega} = \mathbf{S\Omega} \quad (1.3)$$

where $\mathbf{S}$ is a $3 \times M$ beam-steering matrix. If the measurement errors in the radial velocities are σ_ω for all beams, the variances of the velocity component estimates are the diagonal elements of $\mathbf{SS}^T$ times σ_ω^2. Two common examples for $M = 3$ systems are (i) $\theta_1 = \theta_2 = \theta$, $\theta_3 = 0°$, $\phi_1 = 0°$, and $\phi_2 = 90°$, and (ii) $\theta_1 = \theta_2 = \theta_3 = \theta$, $\phi_1 = 0°$, $\phi_2 = 120°$ and $\phi_3 = 240°$. For example (i) $\sigma_u^2 = \sigma_\omega^2(1 + \cos^2\theta)/\sin^2\theta$ and for example (ii) $\sigma_u^2 = \sigma_\omega^2 2/(3\sin^2\theta)$, and in general the errors due to measurement error increase steeply as θ becomes smaller.

However, errors due to spatial inhomogeneity increase as θ gets larger, since the horizontal separation of sampling volumes at a height z are, for case (i), $z\tan\theta$, $z\tan\theta$, and $2^{1/2}z\tan\theta$, and for case (ii), all $3^{1/2}z\tan\theta$. As a guide, the longitudinal velocity component structure function $\langle[u(z\tan\theta) - u(0)]^2\rangle \approx 2(\varepsilon z\tan\theta)^{2/3}$ where the eddy dissipation rate ε is typically 10^{-3} m^{2}s^{-3} (Kaimal, 1973), so the rms difference in u over a distance of $ztan\theta$ = 45 m (corresponding to say z = 140 m and θ = 18 °) would be 0.25 m^{2}s^{-2} due to turbulent fluctuations.

For the reasons above, a compromise zenith angle of θ = 15 °–20 ° is used in all commercial sodars. This works reasonably above relatively homogeneous terrain, but is very questionable in the urban boundary layer where, in addition to fluctuating differences in velocity components in the sodar sampling volumes, there may also be systematic differences. Considerable attention has been paid in the literature to remote sensing above

*Corresponding author: Stuart Bradley, University of Auckland, Private Bag 92019, Auckland 1142, New Zealand, e-mail: s.bradley@auckland.ac.nz

forest and hill sites, since these also have inhomogeneous flow above them (Bradley 2012; Bingöl et al., 2009; Behrens et al. 2012; Bradley et al. 2012b). There are two basic approaches to improve remotely sensed winds in such situations. The first approach is to use a flow model to predict corrections to remote sensing data (Bradley, 2012; Bezault et al., 2012). Note that the current state of flow models is not sufficiently sophisticated so that they can be used alone for predicting winds over complex sites (Bechmann et al., 2011). Moreover, urban spatial scales and resulting flow structure is generally much more complex than flow over forests or hills (Drew et al. 2013; Barlow, 2014), so that suitable flow models to correct remote sensing data do not exist. The second approach is to obtain the three vector wind components from a single volume at each height, rather than from spatially distributed volumes. These methods include the WindScanner project (Mikkelsen, 2014), which uses three lidar wind systems, and a bi-static sodar, which uses three acoustic wind systems (Bradley et al., 2012a). However, finding three suitable secure and appropriately spaced sites in an urban area can be a considerable challenge. Therefore, in this work we describe a new instrument which uses a single installation. This necessitates decreasing θ, so that the sampling is more columnar, but also avoiding the error magnification due to large diagonal elements of $\mathbf{S}\mathbf{S}^T$. The method described here is aimed at obtaining a useful compromise between these competing effects.

2 Design concept

The design concept is to increase the number of microphones while decreasing the sensitive cone angle. We can generalize the common example (ii) discussed above by having M microphones, all with zenith angle θ. The radial velocity recorded by the m^{th} microphone is

$$\omega_m = (u + u'_m)\sin\theta\cos\phi_m + (v + v'_m)\sin\theta\sin\phi_m + (w + w'_m)\cos\theta + e_m \quad (2.1)$$

where $\phi_m = 2\pi m/M$, e_m is a random measurement error distributed according to a Gaussian distribution having zero mean and standard deviation σ_e, and (u'_m, v'_m, w'_m) are the turbulent fluctuations in wind vector components at the m^{th} sampling volume.

The wind vector components can be estimated from

$$\hat{u} = \frac{2}{M\sin\theta}\sum_{m=0}^{M-1}\omega_m\cos\phi_m$$
$$\hat{v} = \frac{2}{M\sin\theta}\sum_{m=0}^{M-1}\omega_m\sin\phi_m\,. \quad (2.2)$$
$$\hat{w} = \frac{1}{M\cos\theta}\sum_{m=0}^{M-1}\omega_m$$

Making use of the following

$$\frac{2}{M}\sum_{m=0}^{M-1}\cos^2\phi_m = \frac{2}{M}\sum_{m=0}^{M-1}\sin^2\phi_m = 1$$
$$\frac{2}{M}\sum_{m=0}^{M-1}\cos\phi_m = \frac{2}{M}\sum_{m=0}^{M-1}\sin\phi_m = \frac{2}{M}\sum_{m=0}^{M-1}\sin\phi_m\cos\phi_m = 0$$
$$\frac{2}{M}\sum_{m=0}^{M-1}\sin^2\phi_m\cos^2\phi_m = \frac{1}{4}$$
$$\frac{2}{M}\sum_{m=0}^{M-1}\sin^4\phi_m = \frac{2}{M}\sum_{m=0}^{M-1}\cos^4\phi_m = \frac{3}{4}$$

gives, from (2.1) and (2.2),

$$\sigma^2_{\hat{u}} = \frac{3}{2M}\sigma^2_u + \frac{1}{2M}\sigma^2_v + \frac{2}{M\tan^2\theta}\sigma^2_w + \frac{2}{M\sin^2\theta}\sigma^2_e$$
$$\sigma^2_{\hat{v}} = \frac{1}{2M}\sigma^2_u + \frac{3}{2M}\sigma^2_v + \frac{2}{M\tan^2\theta}\sigma^2_w + \frac{2}{M\sin^2\theta}\sigma^2_e$$
$$\sigma^2_{\hat{w}} = \frac{\tan^2\theta}{2M}\sigma^2_u + \frac{\tan^2\theta}{2M}\sigma^2_v + \frac{1}{M}\sigma^2_w + \frac{1}{M\cos^2\theta}\sigma^2_e \quad (2.3)$$

Here it has been assumed that the variances of u'_m, v'_m, w'_m, and e_m are independent of m, and that the quantities σ^2_u, σ^2_v, and σ^2_w are the variances which would be obtained from repeatedly sampling any of the M spatially distributed volumes. This is only true if the sampling volumes are close together. These volumes are usually sampled sequentially, at times separated by $2z_{\max}/c$, where $z_{\max}$ is the maximum height and c the speed of sound. The variances can be expected to increase as the intervening time increases (Bradley, 2013). One possible model is

$$\sigma^2_{u,m}(t + \Delta t) = \rho^2(\Delta t)\sigma^2_{u,m}(t) + \sigma^2_m[1 - \rho^2(\Delta t)] \quad (2.4)$$

where ρ is a correlation term and σ_m is a random contribution. An exponential dependence on time is assumed so

$$\rho(\Delta t) = \mathrm{e}^{-\Delta t/\tau} \quad (2.5)$$

where τ is the integral time scale. The time Δt taken to obtain each atmospheric profile is generally considerably shorter than τ, but the combined $M\Delta t$ could readily be larger than τ. If we assume $\Delta t \gg \tau$, and that $\sigma^2_u \approx \sigma^2_v \approx \sigma^2_w$,

$$\sigma^2_{\hat{u}} = \frac{2(\sigma^2_u + \sigma^2_e)}{M\sin^2\theta}. \quad (2.6)$$

If the sampling volumes are much closer than the spatial coherence length, then

$$\sigma^2_{\hat{u}} = \frac{2[2(\varepsilon z\tan\theta)^{2/3} + \sigma^2_e]}{M\sin^2\theta}. \quad (2.7)$$

The velocity component estimation errors then depend on the relative contributions from the longitudinal velocity component structure function and the variance of the measurement error. Therefore, for small $z\tan\theta$, the significant geometric design parameter is $M\sin^2\theta$, and for large $z\tan\theta$ the significant geometric design parameter is $M\sin^{4/3}\theta$. In the small $z\tan\theta$ case, a similar velocity component error will be incurred with $\theta = 11\,^\circ$ and $M = 8$, or $\theta = 8\,^\circ$ and $M = 16$, as for $\theta = 18\,^\circ$ and $M = 3$. In the large $z\tan\theta$ case, a similar error will be incurred with $\theta = 8.5\,^\circ$ and $M = 8$, or $\theta = 5\,^\circ$ and $M = 16$, as for $\theta = 18\,^\circ$ and $M = 3$. Consequently, it should be possible to offset increased velocity component error at small beam zenith angles by increasing the number of acoustic beams used.

Since the multiple beams will be more closely clustered around the zenith, it is also proposed that a single transmitted beam be used, and the M microphones receive backscattered sound from the periphery of the volume filled by the transmitted beam. This has the advantages of a more compact system, and being necessary to transmit only vertically, obtaining vector profiles at a much faster rate. The M microphones can be spaced evenly around a circle of radius r centered on the focus of a parabolic dish of focal length F. The zenith angle for all microphones is then

$$\theta = \tan^{-1}\frac{r}{F}. \tag{2.8}$$

A typical small parabolic satellite dish has $F = 500\,\mathrm{mm}$. For $\theta = 5\,^\circ$ the radial distance of the microphones from the focal point would be $r = 44\,\mathrm{mm}$, and for $\theta = 8\,^\circ$, $r = 68\,\mathrm{mm}$. Initially a horn speaker surrounded by the microphone ring was considered. Suitable horn speakers generally had diameters greater than 150 mm, and so $M = 8$ was chosen, giving an available diameter space for the speaker of 192 mm for the small $z\tan\theta$ case.

The Doppler shift Δf for this configuration is quite small. For $v = 0$, $m = 0$, $u = 1\,\mathrm{ms}^{-1}$, and wavenumber $k = 80\,\mathrm{m}^{-1}$ (nominal frequency 4330 Hz), $\Delta f = ku\sin(11\,^\circ)/\pi = 4.8\,\mathrm{Hz}$. For a $T = 0.05\,\mathrm{s}$ sampling duration, corresponding to a height resolution of $\Delta z = cT/2 = 8.5\,\mathrm{m}$ (with speed of sound $c = 340\,\mathrm{ms}^{-1}$), the spectral bin separation is $1/T = 20\,\mathrm{Hz}$. So the Doppler shift from $1\,\mathrm{ms}^{-1}$ wind is only around 0.24 of the spectral bin separation (compared with 0.4 of the bin separation for $\theta = 18\,^\circ$). This is another reason for choosing $M = 8$ instead of $M = 16$.

Also, the zenith angle subtended by a 10 mm diameter microphone is only $\tan^{-1}(10/510) = 1\,^\circ$ and the scattering volumes sampled by individual microphones are essentially independent. They are all sampled simultaneously, which is a big advantage in obtaining accurate winds, because the entire vector wind is obtained at the same time at each height, in contrast with other remote sensing instruments. The extent of the volume sampled by all microphones, with $\theta = 11\,^\circ$, has a diameter of 39 m, at a range of $z = 100\,\mathrm{m}$, compared with 65 m for $\theta = 18\,^\circ$. There should therefore be a lot less spatial correlation error in the estimated winds. Also, because a single transmitted beam is used, this configuration is much less susceptible to acoustic echoes from fixed objects.

One disadvantage of the design described above is that the single vertically transmitted pulse will have decreased gain at the zenith angle of the microphone ring. This is considered later.

3 Design implementation

Dish reflector considerations: Ray tracing (high frequency) approximation

For $M = 8$ microphones, the microphone ring will have a diameter of nearly 200 mm for $\theta = 11\,^\circ$. If a parabolic dish of focal length $F = 510\,\mathrm{mm}$ is chosen (a commonly available design), then the obstruction arising from the sensor head would be $\pm 11\,^\circ$. Therefore an offset-parabolic dish is chosen (also commonly used for domestic satellite receivers for the same reason). The acoustic beam width from shallow *spherical* dishes has been modelled by Deane (1999). While spherical reflectors exhibit aberrations, they do have the advantage that a focal surface exists, so that placement of off-axis detectors also results in high gain. This is not true for parabolic reflectors, for which placing a detector off-axis can be expected to give rise to a wider beamwidth. Although offset parabolic antennas are commonly used for domestic satellite receivers, and often with multiple feeds, no literature has been identified which describes their off-axis beam patterns. Consequently the following investigates this problem.

The dish surface can be described in Cartesian coordinates by

$$z = \frac{x^2 + y^2}{4F}. \tag{3.1}$$

where the dish axis is in the z direction. A 2D section through the dish along the azimuth ϕ becomes

$$z = \frac{(x\cos\phi + y\sin\phi)^2}{4F} = \frac{x'^2}{4F}. \tag{3.2}$$

The slope of the dish in this direction is

$$\tan\alpha = \frac{dz}{dx'} = \frac{x'}{2F} \tag{3.3}$$

so that the upward surface normal is

$$\mathbf{n} = (-\sin\alpha\cos\phi, -\sin\alpha\sin\phi, \cos\alpha). \tag{3.4}$$

Let the ray from (x, y, z) on the dish surface to the microphone have unit vector $\mathbf{p}$ and the incident ray from turbulent backscatter, which reflects off the dish, have unit vector $\mathbf{r}$. Then the laws of reflection give

$$\begin{aligned} \mathbf{r}\cdot\mathbf{n} &= \underline{\mathbf{p}}\cdot\mathbf{n} \\ \mathbf{n}\times\mathbf{r} &= \mathbf{p}\times\mathbf{n} \end{aligned} \tag{3.5}$$

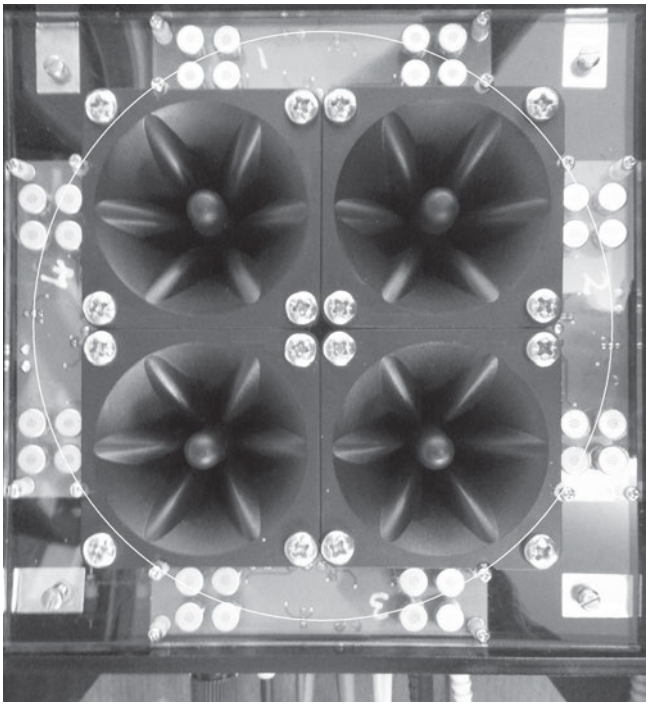

Figure 1: The sensor head unit, showing the four central speakers surrounded by eight clusters, each cluster comprising four microphones. Also shown, is a white dashed circle of diameter 200 mm.

Figure 2: The complete prototype system, without acoustic baffles.

which can be readily solved for the components of **r**. Small increments in the incident azimuth direction and the incident zenith direction define solid angles for which the microphone is sensitive. Integrating these solid angles numerically gives the microphone polar response. This has been done for the dish used in the prototype instrument. This is an offset-parabolic dish of focal length $F = 510$ mm, with the projection of the dish segment onto the x-y plane being a circle of diameter $D = 780$ mm. The microphones are in a circle of radius 105.6 mm centered on the focal point, but with the plane of the microphones tilted to point at the dish center (satellite dish feeds generally point toward the dish center). In practice a cluster of 4 microphones, each of 10 mm diameter, is used at each of the eight microphone locations around the microphone ring, as shown in Figs. 1 and 2.

Dish reflector considerations: Diffraction

For a wavelength $\lambda = 75$ mm and the projected dish diameter $D = 780$ mm, the first diffraction pattern minimum occurs at $\theta = 1.22\lambda/D = 6.8\,^\circ$. This suggests that the width of the transmitted and received beams will be wider than the ray tracing method might suggest. Consequently the beam patterns have been simulated based on Deane (1999). However that treatment was for a spherical reflector described by

$$x^2 + y^2 + (z - 2F)^2 = (2F)^2$$

or, for $z \ll F$,

$$z = \left(\frac{x^2 + y^2}{4F}\right)\left(1 - \frac{x^2 + y^2}{16F^2}\right).$$

This means that the spherical dish should approximate a parabolic dish providing $[D/(4F)]^2 << 1$. In the present case $[D/(4F)]^2 = 0.15$ and over much of the dish the spherical approximation is very good. Deane (1999) treats dishes having circular symmetry around their axis. However, by changing the angular limits so that integrals include only the offset parabola, the beam pattern for on-axis sources can be calculated. Deane (1999) also suggests how off-axis sources can be handled, and we have used this to estimate beam patterns for sources in the plane of the vertical axis and the center line through the dish.

Speaker considerations

In practice it was decided to use four Motorola KSN1005 speakers, as shown in Figs. 1 and 2, since this configuration will give a speaker polar sensitivity pattern peaking at larger zenith angle compared with a single central speaker. These speakers are known to be robust from being used in phased arrays in various commercial sodars. The KSN1005 has a square aperture of sides 85 mm. Four of these speakers fitted closely together and aligned with edges along the x and y axes

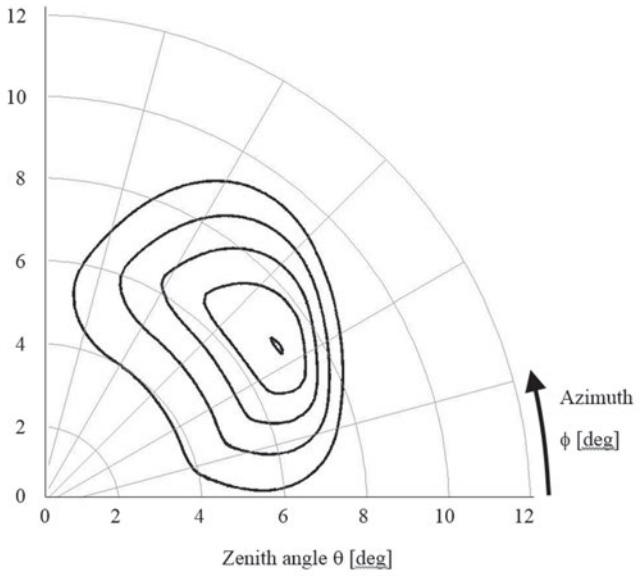

Figure 3: The normalized sound intensity level angular variation for the speakers S1 shown as a projection onto the *x*-*y* plane, with contours at 3 dB intervals.

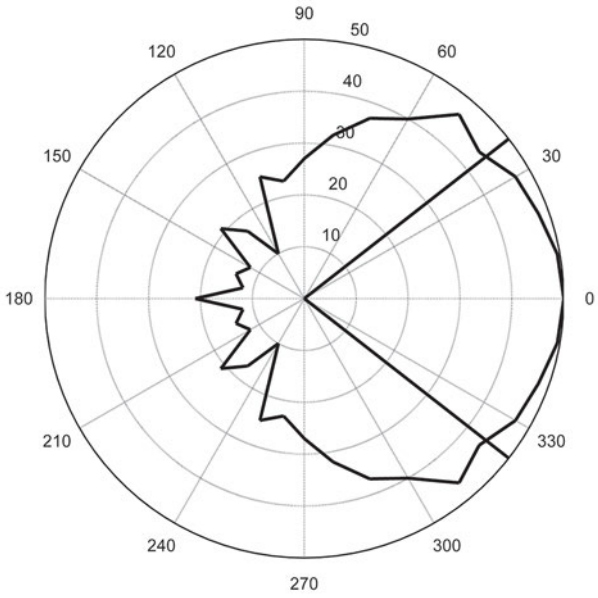

Figure 4: The normalized sound intensity level angular variation of individual speakers. Also shown, as solid lines, are the zenith angle range at $\theta = \pm 38\,^\circ$ for the dish used.

in a rectangular Cartesian coordinate system, allows $M = 8$ microphones equally in a circle at mm coordinates $(85, 85 \times \tan 22.5\,^\circ = 35)$, (35, 85),... This gives radial distances of $r = 92$ mm, or $10\,^\circ$ zenith angle for a $F = 510$ mm dish, although the zenith angles will be larger because of the finite microphone diameters.

The beam pattern of these four speakers combined with the offset parabolic dish has been modelled using the ray tracing method described above. The 85 mm diameter aperture of each speaker was divided into 1800 angular sectors and 100 radial annuli for the integration. The results of the normalized sound intensity level polar response calculation are shown in Fig. 3. The normalized sound intensity level polar response of an isolated speaker, shown in Fig. 4, will affect the outer limits of the speaker/dish response, but does not have any significant effect on the response shown in Fig. 3. Only the response for speaker S1 is shown, since the response for the other speakers are reflections of this plot. Note that projecting the polar beam pattern onto the $x - y$ plane gives the impression of an elliptical beam cross-section. In fact, the following is a good model for the speaker beam pattern

$$G_s(\theta, \phi) = G_{s0} \mathrm{e}^{-\frac{1}{2}\left[\frac{\cos^{-1}(\mathbf{r}\cdot\mathbf{s_0})}{\sigma_s}\right]^2} \qquad (3.6)$$

where $\mathbf{s}_0$ is the unit vector in the direction of the peak response. The peak response is in the direction $\theta_0 = 7\,^\circ$, and $\phi_0 = 35\,^\circ$, being more in the forward direction than $45\,^\circ$ because of the dish being limited in extent in other directions. The estimated angular width is $\sigma_s = 1.8\,^\circ$ and the angular response is shown in Fig. 5.

A full solution to the wave equation is also computed, as described, but assuming a spherical dish, and that the speakers lie in the plane formed by the vertical axis

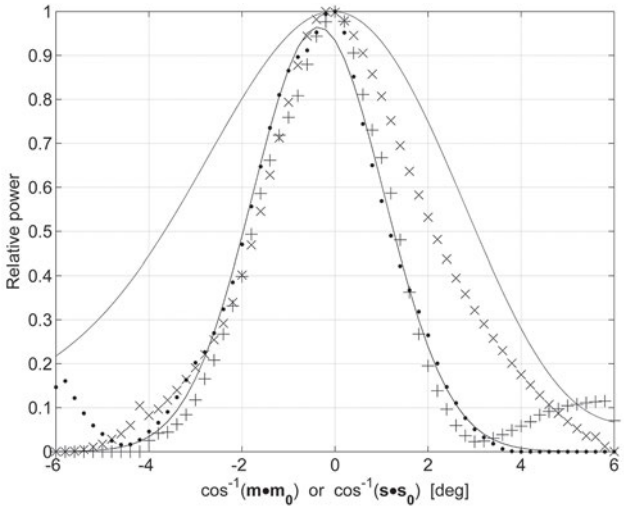

Figure 5: Angular beam patterns with respect to the beam axis for the ray model of M1 (+), the ray model for M2 (•), the gaussian fit to the M2 model (solid line), the ray model for S1 (×), and the full solution for S1, with limitations as discussed (dash line).

and the line through the long dish diameter. Since this model does not inlcude the *y* offset of the speakers, it is not able to locate the beam pattern axis correctly. Nevertheless, this model gives information about the angular width of the beams. For all speakers it is found that the beam pattern using the modified Dean method very closely matches the diffraction pattern based on a disk of diamater *D*. This means the speaker beam pattern has an angular width of $\sigma_s = 3.2\,^\circ$, which is much greater than the ray model predicts. This angular reponse is also shown in Fig. 5.

Microphone considerations

For this design the electret EM172 microphone was used since, in addition to being low-noise and physically small (10 mm diameter), it is omnidirectional, which is desirable for the wide angle subtended at the dish focus by the dish edges for the dish described above. The EM172 microphone has a sensitivity of 38 mV/Pa and self-noise sound pressure level of 14 dBA (dB-SPL A-weighted). A typical sound intensity at a sodar receiver is $10^{-13}\,\mathrm{Wm}^{-2}$ for sound from 100 m (Bradley, 2007), but this is for a speaker array comprising typically 32 speakers, whereas here only 4 such speakers are being used and the power output will be around an order of magnitude smaller. The acoustic impedance of air is about $Z = 400\,\mathrm{Nsm}^{-3}$ so the acoustic pressure corresponding to this sound intensity is about $(400 \times 10^{-14})^{1/2} = 2\,\mu\mathrm{Pa}$ (or -20 dB-SPL). For a parabolic dish of diameter 510 mm and a microphone of diameter 10 mm, the ideal antenna gain (from all acoustic power on the antenna being focused onto the microphone) is $(510/10)^2 = 2600$. Each microphone will ideally produce an output voltage of about 2600×0.038 x $2 \times 10^{-6} = 200\,\mu\mathrm{Vrms}$. The self-noise is $(20\,\mu\mathrm{Pa})\ 10^{14/20} = 100\,\mu\mathrm{Pa}$, producing a noise voltage of $(38\,\mathrm{mV/Pa})(10^{-4}\,\mathrm{Pa}) = 4\,\mu$ Vrms. In practice this random noise could be expected to be distributed quite flatly across 10 kHz or more bandwidth. For a microphone preamplifier circuit bandwidth of, say, 1 kHz, the noise from a single microphone will be 0.4 µVrms, giving a 100 m SNR of $200/0.4 = 500$ in amplitude, or 54 dB.

Naturally, there are other sources of noise, and the above analysis is also very idealized, since not all sound impinging on the dish will reach each microphone. Consequently, it was decided to use a cluster of four such microphones at each of the eight design positions. This increases signal levels by a factor of 4 while increasing uncorrelated noise by only a factor of 2, so the overall signal-to-noise ratio (SNR) is increased by a factor of 2.

The beam pattern of these eight clusters has been modelled, with each of the 10 mm microphones also being split into 225 angular segments and 16 radial annuli. The results of the polar response calculation are shown in Fig. 6. The peak sensitivity for one cluster is at zenith angle $\theta_0 = 9.05\,^\circ$ and azimuth angle $\phi_0 = 24.7\,^\circ$ and, for the other cluster shown, $\theta_0 = 9.46\,^\circ$ and azimuth angle $\phi_0 = 69.9\,^\circ$. Again, the response can be modelled with a Gaussian beam

$$G_m(\theta,\phi) = G_{m0}\mathrm{e}^{-\frac{1}{2}\left[\frac{\cos^{-1}(\mathbf{r}\cdot\mathbf{m_0})}{\sigma_m}\right]^2} \tag{3.7}$$

where $\mathbf{m}_0$ is the unit vector in the direction of the peak response. The estimated angular width is $\sigma_m = 1.32\,^\circ$ and the angular response is also shown in Fig. 5.

The full solution, with the limitations discussed above, is also computed for the microphones. Again, it is found that the angular width is wider than predicted by the ray model, as might be expected given the inclusion of diffraction, as is also shown in Fig. 5.

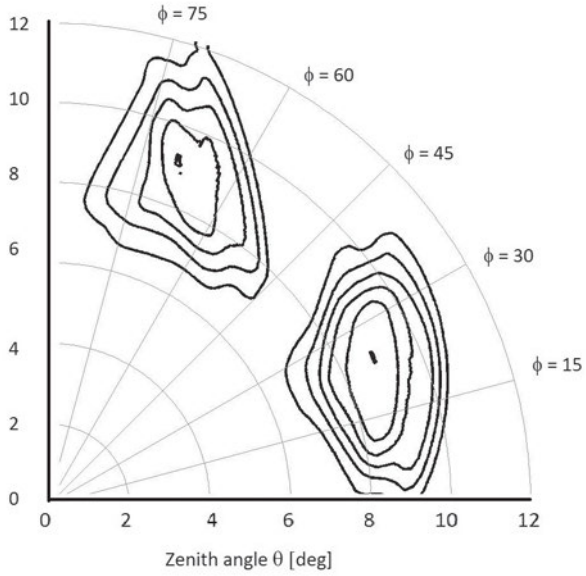

Figure 6: The normalized sound intensity level angular variation for the microphones M1 and M2 shown as a projection onto the *x*-*y* plane, with contours at 3 dB intervals.

Combined beam pattern

The effect of the dish is to give quite tight focus to both speakers and microphones. Since the speaker centers and the microphone centers are at different radial distances from the dish axis, and because there are 4 speakers and 8 microphones, their beam patterns do not coincide. The effect of the more centralized speaker pattern is to move the peaks toward smaller zenith angles (around 8 °) and closer to the $\phi = \pm 45\,^\circ$ and $\pm 135\,^\circ$ radials. The combined beam pattern is proportional to

$$\begin{aligned}
G_c(\theta,\phi) &= G_{s0}G_{m0}\mathrm{e}^{-\frac{1}{2}\left[\frac{\cos^{-1}(\mathbf{r}\cdot\mathbf{s_0})}{\sigma_s}\right]^2}\mathrm{e}^{-\frac{1}{2}\left[\frac{\cos^{-1}(\mathbf{r}\cdot\mathbf{m_0})}{\sigma_m}\right]^2} \\
&\approx G_{s0}G_{m0}\mathrm{e}^{-\frac{1}{2\sigma_s^2}(\mathbf{r}-\mathbf{s_0})\cdot(\mathbf{r}-\mathbf{s_0})}\mathrm{e}^{-\frac{1}{2\sigma_m^2}(\mathbf{r}-\mathbf{m_0})\cdot(\mathbf{r}-\mathbf{m_0})} \\
&\approx G_{s0}G_{m0}\mathrm{e}^{-\left(\frac{1}{\sigma_s^2}+\frac{1}{\sigma_m^2}\right)}\mathrm{e}^{\mathbf{r}\cdot\left(\frac{\mathbf{m_0}}{\sigma_m^2}+\frac{\mathbf{s_0}}{\sigma_s^2}\right)} \\
&\approx G_{s0}G_{m0}\mathrm{e}^{-\left(\frac{1}{\sigma_s^2}+\frac{1}{\sigma_m^2}\right)}\mathrm{e}^{\mathbf{r}\cdot\frac{\mathbf{c_0}}{\sigma_c^2}} \\
&= G_{c0}\mathrm{e}^{-\frac{1}{2}\left[\frac{\cos^{-1}(\mathbf{r}\cdot\mathbf{c_0})}{\sigma_c}\right]^2}
\end{aligned} \tag{3.8}$$

where

$$\frac{1}{\sigma_c^4} = \frac{1}{\sigma_s^4} + \frac{1}{\sigma_m^4} + 2\frac{\mathbf{s_0}\cdot\mathbf{m_0}}{\sigma_s^2\sigma_m^2}$$

$$\mathbf{c_0} = \sigma_c^2\left(\frac{\mathbf{m_0}}{\sigma_m^2} + \frac{\mathbf{s_0}}{\sigma_s^2}\right) = \frac{\frac{\mathbf{m_0}}{\sigma_m^2} + \frac{\mathbf{s_0}}{\sigma_s^2}}{\left|\frac{\mathbf{m_0}}{\sigma_m^2} + \frac{\mathbf{s_0}}{\sigma_s^2}\right|}.$$

The unit vector, $\mathbf{c}_0$, is a variance-weighted location between the position, $\mathbf{s}_0$, of the peak speaker response and

the position, $\mathbf{m}_0$, of the peak microphone response. The peak response occurs at $\mathbf{r} = \mathbf{c}_0$. If $\sigma_M = \sigma_S$ then the peak is at the midpoint of the speaker and microphone peaks. If $\sigma_M > \sigma_S$ then the peak is closer to the postion of the peak speaker response.

The assumption of a constant zenith angle, used in (2.1) and (2.2), is reasonable, with $\theta = 8\,^\circ$ and a zenith angle half-power half-beam-width $2.3\,^\circ$ being a good fit. However, the best fit to the azimuth angles of the combined beams are $\pm 29\,^\circ$, $\pm 61\,^\circ$, $\pm 119\,^\circ$, and $\pm 151\,^\circ$.

4 Wind drift

During the course of the transmitted sound wave travelling upward to the scattering volume and back down to be received by the microphones, the sound wave will also move with the wind. This wind drift has recently been the subject of an investigation by Bradley and Strehz (2014) for the case where the transmitter beam axis and the receiver beam axis coincide. They concluded that, except for the possible effect of acoustic baffles, a sodar with identical transmitter and receiver beams is self-compensating for wind drift Doppler shift errors. However, in the current design the transmitter (speaker) beam patterns are centered on a different direction from the receiver (microphone) beam patterns. If wind drift is taken into consideration, and for small zenith angles, reception from direction $\mathbf{r}$ is due to scattering from sound initially transmitted in direction $\mathbf{r} - 2\mathbf{V}/c$ upstream corresponding to translation of the transmitted sound due to the wind for the time taken from transmission to reception. Repeating the calculation of the previous section, but with this extra translation of the speaker beam, the peak response occurs at

$$\mathbf{c'_0} = \frac{\frac{\mathbf{m_0}}{\sigma_m^2} + \frac{\mathbf{s_0}}{\sigma_s^2} + \left(\frac{1}{\sigma_m^2} + \frac{1}{\sigma_s^2}\right)\frac{\mathbf{V}}{c}}{\left|\frac{\mathbf{m_0}}{\sigma_m^2} + \frac{\mathbf{s_0}}{\sigma_s^2} + \left(\frac{1}{\sigma_m^2} + \frac{1}{\sigma_s^2}\right)\frac{\mathbf{V}}{c}\right|} \tag{4.1}$$

The radial velocity component is from Doppler shift from the transmitted energy travelling in direction $\mathbf{c'_0} - \frac{\mathbf{V}}{c}$ which is scattered into direction $-\left(\mathbf{c'_0} + \frac{\mathbf{V}}{c}\right)$ so that the radial velocity component is

$$\begin{aligned} \omega' &= \mathbf{V} \cdot \mathbf{c'}_0 \\ &\approx \omega + \sigma_c^2 \left(\frac{1}{\sigma_m^2} + \frac{1}{\sigma_s^2}\right)\frac{V^2}{c}. \end{aligned} \tag{4.2}$$

For $\sigma_m = \sigma_s$, $\omega' \approx \omega + \frac{V^2}{c}$. Referring to (2.2), the effect on $\hat{u}$ and $\hat{v}$ should be minor, providing the signal levels do not decrease too much, but the estimate of the vertical velocity component should now be

$$\begin{aligned} \hat{w} &= \frac{1}{M\cos\theta}\sum_{m=0}^{M-1}\omega'_m - \frac{V^2}{c\cos\theta} \\ &\approx \frac{1}{M\cos\theta}\sum_{m=0}^{M-1}\omega'_m - \frac{\hat{u}^2 + \hat{v}^2}{c\cos\theta}. \end{aligned} \tag{4.3}$$

5 Preliminary tests

The transmitter frequency was $f_T = 4500$ Hz and pulses of duration 100 ms were transmitted (about 17 m vertical resolution). Received signals were recorded at a sampling rate of $f_s = 32768$ Hz for a duration of 3 s for each profile. In order to examine the signal strength in the time domain, time gating of 2 ms was used (about 9 cycles of 4500 Hz), corresponding to 1/3 m in space. The mean-squared value, P, of the received signal was found for each time gated sample. This includes the sinusoidal signal received plus random noise, and could be modelled via the sodar equation (Bradley 2007) as

$$P = P_0 \frac{\mathrm{e}^{-2az}}{z^2} + \sigma_n^2 \tag{5.1}$$

where P_0 is proportional to the scattering cross section within a range gate, z is height, a is the acoustic absorption index, and σ_n^2 is the noise variance (assumed constant). The SNR is

$$\mathrm{SNR} = b\frac{P_0}{\sigma_n^2}\frac{\mathrm{e}^{-2az}}{z^2} = b\frac{P - \sigma_n^2}{\sigma_n^2}. \tag{5.2}$$

where b is included to allow for a possible difference between the bandwidth of the noise compared to that of the signal. The noise variance is estimated from the topmost part of each profile (i.e. for large z) and then, assuming P_0 and α are independent of height z, P_0 and α are found from a linear fit using $\ln[(P - \sigma_n^2)z^2] = \ln(P_0) - 2az$. Estimation of a in this way is a useful check, since typical values are known, although of course scattering cross section does change with height depending on thermal turbulence strength, and absorption changes with height depending on atmospheric thermodynamic properties. The resulting profiles of SNR allow an estimate to be made of the height to which useful data might be obtained, as well as a method of detecting anomalous behaviour. The model based on (5.1) does not account for echoes from fixed objects though, so the results are a little biased. Also, the height at which SNR = 1 is extremely conservative, since no signal processing (such as spectral peak detection) has been used. Fig. 7 shows a typical SNR profile, together with the linear fit, where the signals and noise have been averaged over 10 minutes and over all eight microphones. The increase in random noise for SNR < 0 dB is obvious. Also there is a significant echo from a building at a distance of about 50 m, and a smaller echo from a distance of 65 m. From a small sample of 100 ten-minute averages, 99 % of the heights where SNR ≤ 0 dB were above 110 m and 17 % above 150 m. The absorption coefficient a estimated in the height ranges of 35–45 m and 80–100 m is 0.15 dB m^{-1}, whereas at this operating frequency values less than 0.1 dB m^{-1} would be expected. This increased signal loss with height is likely due to the wind drift, which is not included in (5.2).

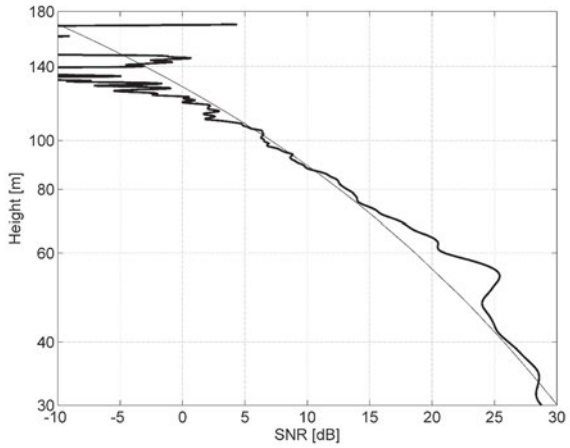

Figure 7: Signal-to-noise ratio as a function of height for a typical profile averaged over all microphones and over a period of 10-minutes.

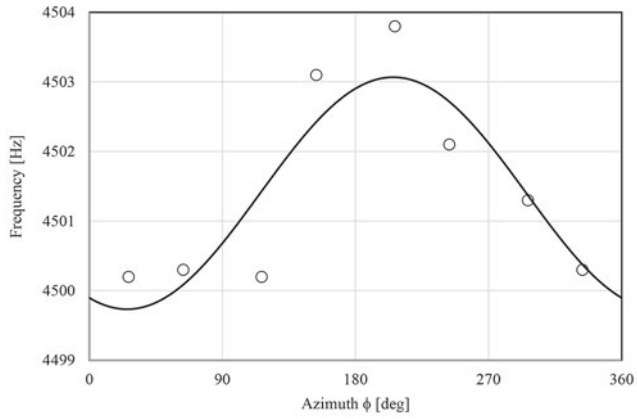

Figure 9: The normalized Doppler shift from the peak of the Gaussian fit to the spectra for the eight microphones. Data corresponding to Fig. 8 are shown as circles, and a sinusoid fit shown as a solid line.

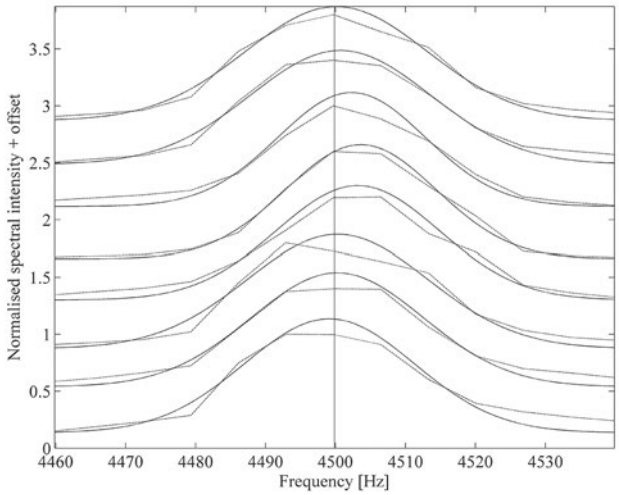

Figure 8: Spectra from the eight microphones at 80 m for a 10-minute average (dashed lines). The smooth solid lines show Gaussian fits to the spectra. Spectra are shown with vertical offsets for clarity.

6 First experimental results

First measurements were conducted at the University of Reading Meteorological Station, where data was available from a sonic anemometer mounted at 10 m. Fig. 8 shows an example of spectra obtained from a 20 m range gate centered on 80 m height using a pulse duration of 0.1 s. The characteristic sinusoidal variation of the spectral peak with microphone position is evident. Fig. 9 shows the corresponding spectral peak frequencies. The estimated wind direction is 194 ° based on (2.2). The estimated direction for the following 10 minute period is 177 °. The standard deviation of the estimate of the phase angle for the sinusoid fit was 18 ° for this data set. However, the 10 m mast data 5-minute averages were 4.8 m s^{-1}, 181 ° and 4.6 m s^{-1}, 212 ° for the first 10 minute period, and 5.2 m s^{-1}, 168 ° and 4.6 m s^{-1}, 183 ° for the second 10-minute period. Simply averaging directions for each pair of 5-minute mast data gives 197 ° and 176 °, showing the direction turning by 11 ° during this period. While the spectral width of the spectra shown in Fig. 9 is as expected from the transmitted pulse length, the Doppler shifts are much smaller than expected based on a beam zenith angle of 8 °. The vertical velocity estimated from (2.2) is $\hat{w} = 0.05\,\mathrm{ms}^{-1}$. Using (2.2) to estimate $\hat{u}\sin\theta$ and $\hat{v}\sin\theta$, an estimate of the radial wind speed $\hat{V}\sin\theta$is obtained. Based on the wind speed of 4.8 m s^{-1} recorded at 10 m, with no correction for height, the zenith angle θ would be around 1 °. This suggests that the calculated beam patterns are not correct, or the wind drift effects are much more dominant than estimated.

A number of short records were recorded of 10 minute average winds from the sodar and from a sonic anemometer at 10 m height. Fig. 10 shows a comparison for the longest of these records (3 hour 40 minutes) assuming a zenith angle θ of 1.2 °. The correlation is poor (correlation coefficient $R = 0.6$). Undoubtedly some of this poor correlation is due to the fact that the comparison is over a short time period, between a 10 m wind and an 80 m wind, and the 10 m mast site has buildings on two sides and trees on the other two sides. Nevertheless, individual measurements such as those shown in Fig. 9 are rather noisy, and it is likely that a considerable amount of fluctuation in Fig. 10 derives from signal noise.

7 Discussion

The concept for this new design is relatively simple: a single vertical sound beam and a circle of microphones around the edges of that beam, thereby reducing the spatial spread of sampling volumes and also allowing for more rapid profiling. However, the beam design is not

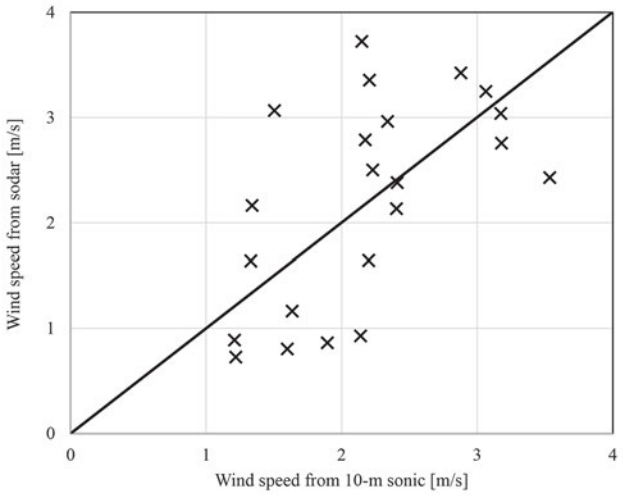

Figure 10: Comparison between 10 minute average winds from the sodar at 80 m height, and from a sonic anemometer at 10 m height, during a 3 hour 40 minutes period. A 1:1 solid line is also shown.

trivial. Firstly, using a single central transmitted beam means that it is difficult to overlap the receiver beams adequately, unless separated transmitter and receiver antennas are used, or some type of half-transparent reflector is employed (similar to an optical beam-splitter). Neither of these options was considered attractive, so a single transmitter/receiver head unit was used together with a parabolic dish antenna. A single speaker could have been used, but it was decided to attempt to better overlap the speaker and receiver beams through using four speakers. In practice this most likely resulted in each microphone only being effectively influenced by the transmitted power from a single speaker, and so the signal strength was generally not high. However, an analysis of spherical spreading loss indicates that transmitted signals are received from at least 120 m height, which is probably adequate for the intended purpose as an urban wind profiler. Although parabolic dish antennas with multiple signal feeds are routinely used in domestic satellite television, the design of a multiple feed acoustic dish antenna was more complicated than expected. Both ray tracing and approximation by a spherical reflector were used, but an optimized design would need both a simulation model for the full acoustic performance of an offset parabola dish, and far-field beam evaluation through measurements (for this prototype, near field measurements of the beam pattern did not give sensible results and an echo-free space of sufficient size for far field measurements was not found). The multiple speaker arrangement biases the sampling volume azimuth locations away from a regular angular spacing, although this was not found to be a serious shortcoming.

Early in the development if was realized that beam drift, or advection of the transmitted beam downstream, was a likely problem. This has been evaluated and, to first order it appears that there should be little impact on Doppler shift, although a likely major impact on signal strength. This can be seen in a greater than expected signal loss with height in Fig. 7, as well as the problems experienced with echos from surrounding hard objects.

The prototype instrument was evaluated at a field station and comparisons made with measurements from a sonic anemometer mounted on a 10 m mast. The expected cosine dependence on microphone azimuth sensitivity was observed, and the wind direction dependence. However, the Doppler shifts observed were very much smaller than predicted by the beam analysis. This suggests that the receiver beam zenith angles were close to 1 ° rather than 8 °, which is a very large discrepancy. Assuming this zenith angle, some comparisons were made between sodar winds at 80 m and sonic winds at 10 m. The correlation is relatively weak (in comparison with that expected from a conventional sodar, for example) although the site was not ideal and the volumes sampled by the two instruments were at very different heights. Nevertheless, it is clear that the new sodar is recording winds in a manner similar to that expected. The correlation of wind directions would appear to be more robust to the wind drift error.

The unexpectedly small zenith angle means that the arguments leading to the choice of $M = 8$ microphones are invalid, and the signal-to-noise ratio for the new sodar can be expected to be considerably worse than that of a conventional sodar. There are two possible explanations for the small zenith angle. The first is that the speaker beam pattern is more closely confined to the zenith direction than estimated in the beam analysis. A mechanism for this would be if the whole 4-speaker assembly acts as a resonating surface rather than as four independent speakers. The second possible explanation for the small zenith angle is that the approximations made in the beam modelling are inadequate, and both the transmitter and receiver beams are more closely confined to the zenith direction. This explanation seems less likely though.

In conclusion, while the overall concept of the design appeared attractive, this new instrument cannot be considered as a useful replacement for conventional sodars without considerable redesign. In particular, the design aim of receiver zenith angles of around 8 ° needs to be achieved somehow, but this is likely to require a completely different antenna configuration.

Acknowledgements

Thanks to Rosy Wilson, Andrew Lomas, and Dawn Turner for technical and logistics support, and to EPSRC EP/G029938/1 for funding.

References

Barlow, J.F., 2014: Progress in observing and modelling the urban boundary layer. Urban Climate **10**, 216–240.

Bechmann, A., N.N. Sørensen, J. Berg, J. Mann, P.-E. Réthoré, 2011: The Bolund experiment, part II: blind comparison of microscale flow models. – Bound.-Layer Meteor. **141**, 245–271.

Behrens, P., J. O'Sullivan, R. Archer, S. Bradley, 2012: Underestimation of monostatic sodar measurements in complex terrain. – Bound.-Layer Meteor. **143**, 97–106.

Bezault, C., S. Sanquer, M. Nadah, 2012: Correction tool for Lidar in complex terrain based on CFD outputs. – Proceedings, EWEA, Copenhagen April, 1276–1282, ISBN: 978-1-62748-291-2.

Bingöl, F., J. Mann, D. Foussekis, 2009: Conically scanning lidar error in complex terrain. – Meteorol. Z. **18**, 189–195.

Bradley, S., 2007: Atmospheric Acoustic Remote Sensing: Principles and Applications. – CRC Press.

Bradley, S., 2012: A simple model for correcting sodar and lidar errors in complex terrain. – J. Atmos. Ocean. Technol. **29**, 1717–1722.

Bradley, S., 2013: Aspects of the correlation between sodar and mast instrument winds. – J. Atmos. Ocean. Technol. **30**, 2241–2247.

Bradley, S., A. Strehz, 2014: Corrections to sodar Doppler winds due to wind drift. – Meteorol. Z., **24**, 605–614, DOI:10.1127/metz/2014/0627.

Bradley, S., S. von Hünerbein, T. Mikkelsen, 2012a: A Bistatic Sodar for Precision Wind Profiling in Complex Terrain. – J. Atmos. Ocean. Technol. **29**, 1052–1061.

Bradley, S., Y. Perrott, P. Behrens, A. Oldroyd, 2012b: Corrections for wind-speed errors from sodar and lidar in complex terrain. – Bound.-Layer Meteor. **143**, 37–48.

Deane, G.B., 1999: The beam forming properties of a concave spherical reflector with an on-axis receiver. – J. Acoust. Soc. Ameri. **106**, 1255–1261.

Drew, D.R., J.F. Barlow, S.E. Lane, 2013: Observations of wind speed profiles over Greater London, UK, using a Doppler lidar. – J. Wind Eng. Ind. Aerodyn. **121**, 98–105.

Kaimal, J.C., 1973: Turbulenece spectra, length scales and structure parameters in the stable surface layer. – Bound.-Layer Meteor. **4**, 289–309.

Mikkelsen, T., 2014: Lidar-based Research and Innovation at DTU Wind Energy – A Review. – J. Phys. Conference Series 524, 012007.